

Slim Disk: Viscosity Prescriptions and Observational Implications

Ken-ya WATARAI

Department of Astronomy, Graduate School of Science, Kyoto University, Sakyo-ku, Kyoto 606-8502
watarai@kusastro.kyoto-u.ac.jp

Shin MINESHIGE

Yukawa Institute for Theoretical Physics, Kyoto University, Sakyo-ku, Kyoto 606-8502
mineshige@yukawa.kyoto-u.ac.jp

(Received 2001 February 28; accepted 2001 August 14)

Abstract

We examine the effects of the different viscosity prescriptions and the magnitude of the viscosity parameter, α , on the structure of the slim disk, and discuss the observational implications on accretion-flow structure into a stellar-mass black hole. In contrast with a standard disk, in which the “ α ” value does not affect significantly the local flux, radiation from the slim disk is influenced by the α value. For the range of $\alpha = 10^{-2} \sim 10^0$ we calculate the disk spectra and from spectral fitting we derive $T_{\text{in}}^{\text{obs}}$, maximum temperature of the disk, $R_{\text{in}}^{\text{obs}}$, the size of the region emitting blackbody radiation with $T_{\text{in}}^{\text{obs}}$, and $p \equiv -\text{dln}T_{\text{eff}}/\text{dln} r$, the slope of the effective temperature distribution. It was founded that the estimated $T_{\text{in}}^{\text{obs}}$ slightly increases as α increases. This is because the larger the magnitude of viscosity is, the larger becomes the accretion velocity and, hence, the more enhanced becomes advective energy transport, which means less efficient radiative cooling and thus higher temperatures.

Furthermore we check different viscosity prescriptions with the form of the viscous stress tensor of $t_{r\varphi} = -\alpha\beta^\mu p_{\text{total}}$, where β is the ratio of gas pressure (p_{gas}) to total pressure, $p_{\text{total}} (= p_{\text{gas}} + p_{\text{rad}})$, and μ is a parameter ($0 \leq \mu \leq 1$). For $\mu = 0$ we have previously found that as luminosity approaches the Eddington, $L_E, R_{\text{in}}^{\text{obs}}$ decreases below $3r_g$ ($3r_g$ corresponds to the radius of the marginally stable circular orbit, r_{ms} , with r_g being Schwarzschild radius) and the effective temperature profile becomes flatter, $T_{\text{eff}} \propto r^{-1/2}$. Such a slim-disk nature does not appear when μ is large, $\mu \sim 0.5$, even at the Eddington luminosity. Hence, the temperature of the innermost region of the disk sensitively depends on the μ value. We can rule out the case with large μ (~ 0.5), since it will not be able to produce a drop in $R_{\text{in}}^{\text{obs}}$ with an increase in luminosity as was observed in an ultraluminous X-ray source, IC 342, source 1.

Key words: accretion: accretion disks, black holes—stars: X-rays

1. Introduction

The accretion disk model by Shakura and Sunyaev (1973, hereafter, SSD) has been regarded as the “standard” model for the low mass X-ray Binaries (LMXBs) and galactic black-hole candidates (GBHCs) in their soft state. Their analytical solutions are self-consistent under some specific assumptions. However, when its luminosity L approaches the Eddington luminosity, L_E , some assumptions break down and thus the standard model cannot adequately describe the nature of such high luminosity objects. The critical luminosity is $L \sim 0.3L_E$ (Abramowicz et al. 1988, Laor, Netzer 1989). This fact is theoretically established but not widely known and still most of investigations have been conducted by simply applying the canonical SSD even to near-Eddington luminosity systems without any comments.

Recent observations have detected several kinds of exotic super-Eddington sources, whose luminosity seemingly exceeds the Eddington luminosity. The properties of their energy source cannot be described by the SSD theory, and hence its origin is still an open astrophysical question. The nature of super-Eddington sources has been

discussed in relation to their X-ray properties since late 1980’s (Fabbiano, 1989). For instance, Ultra-Luminous Compact X-ray Sources (hereafter, ULXs) in nearby spiral galaxies are very mysterious objects. Their luminosities amount to around $10^{39-40} \text{erg s}^{-1}$, which means the mass (M) of black holes, if they exist, should exceed 10–100 M_\odot . However, the MCD (multi-color disk, Mitsuda et al. 1984) fitting derives relatively high temperatures, $T_{\text{in}}^{\text{obs}} \simeq 1.0 - 2.0 \text{ keV}$ (Mizuno et al. 1999, Makishima et al. 2000), compared with the theoretical expectations based on the SSD model, which is significantly below 1.0 keV for $M \gtrsim 100M_\odot$. Here, $T_{\text{in}}^{\text{obs}}$ is the color temperature derived from the observed spectrum (for the exact definition, see Section 3.3.). In our Galaxy, there exists a famous galactic microquasar, GRS 1915+105, which shows the complicated time/spectral variation. Its luminosity is near the Eddington luminosity in its high state $\gtrsim \text{a few} \times 10^{39} \text{erg s}^{-1}$ (Belloni et al. 2000). These objects can never be explained in the framework of the SSD theory.

On the theoretical side, there has been growing recognition that the super-critical accretion disk model, so-called “slim disk” (Abramowicz et al. 1988) may be a

correct model to describe these high luminosity objects. Its significance has been re-recognized in connection with luminous AGNs (Szuszkiewicz et al. 1996, Wang et al. 1999), narrow-line Seyfert1 galaxies (NLS1s; Mineshige et al. 2000), and GBHCs shining near the Eddington luminosity (Fukue 2000, Watarai et al. 2000), since the disk is stable due to the advective entropy transport, even at the super-critical accretion rates. The ULXs are discussed along this line in the first time by Watarai et al. (2001) and it has been shown to explain the basic observed tendency, although more detailed analysis is needed (Watarai in preparation).

The local stability against thermal perturbations can be discussed in terms of the thermal equilibrium curve, so called ‘‘S-shaped’’ curve (Taam, Lin 1986, Abramowicz et al. 1995). The local stability properties for the stationary slim disk models with different viscosity prescriptions were discussed by Szuszkiewicz (1990), who found that when ‘‘ μ ’’ increases the thermally unstable region in the disk becomes smaller. Here, we prescribe viscous-shear tensor, the different form of shear stress tensor to be, $t_{r\varphi} = -\alpha p_{\text{gas}}^\mu p_{\text{total}}^{1-\mu}$, (p_{gas} is the gas pressure, and p_{total} is the total pressure), where μ is the parameter ($0 \leq \mu \leq 1$).

The global stability analysis for slim disk model has been carried out by Honma et al. (1991) who found that the disk was stabilized as the viscosity parameter ‘‘ μ ’’ increased. Szuszkiewicz and Miller (1997) confirmed this finding, showing that the models are stable not only when they are locally stable but also when the local analysis predicts an unstable region with radial dimension smaller than the shortest wavelength of the unstable modes. In the most recent study by Zampieri et al. (2001) have calculated the spectra of a slim disk model along one full thermal limit cycle. However, there is little research that carried out direct comparison with X-ray observations.

Our concern in the present study is how the viscosity prescription and its strength act on the structure of accretion disks, and how they manifest themselves in the fitting parameters ($T_{\text{in}}^{\text{obs}}$, $R_{\text{in}}^{\text{obs}}$) derived from the observational spectra in soft X-ray band. If $T_{\text{in}}^{\text{obs}}$ and $R_{\text{in}}^{\text{obs}}$ can be accurately determined from the observation, conversely, the functional form of disk viscosity might be able to constrain. A comprehensive understanding of the structure and spectrum of slim disks is an outstanding issue.

In the next section we introduce the basic equations and explain our calculation method. In section 3, the results of our calculation are presented for a variety of viscosity parameters (α, μ). The observational features of the slim disk are summarized by using the fitting parameters, $T_{\text{in}}^{\text{obs}}$, $R_{\text{in}}^{\text{obs}}$, and p in section 4. Final section is devoted to discussion and concluding remarks.

2. Basic Equations

Basic equations we use here are all the same as those in the previous paper (Watarai et al. 2000) except for the viscosity prescription (see Kato et al. 1998, Chapter 8 for the detailed description). We solved the height-integrated equations (Hōshi, 1977) in the radial direction on the basis

of pseudo-Newtonian potential (Paczynsky, Wiita, 1980), and neglected self-gravity. The pseudo-Newtonian potential is not an excellent approximation around the event horizon $\sim r_g$. Thus, caution is needed when the derived $R_{\text{in}}^{\text{obs}}$ is small, $R_{\text{in}}^{\text{obs}} \lesssim r_g$. Other general relativistic effects needs also to take account, then. Otherwise, our approximation does not introduce serious errors.

Honma et al. (1991) were the first to carry out the calculation above circumstances (including the effect of viscosity prescriptions of the slim disk). The main difference of our calculation and theirs is that they truncated the disk inner edge at $2.7 r_g$, while we integrate the disk down to the real vicinity of the event horizon at r_g .

The momentum equation in the radial direction is

$$v_r \frac{dv_r}{dr} + \frac{1}{\Sigma} \frac{dW}{dr} = \frac{\ell^2 - \ell_K^2}{r^3} - \frac{W}{\Sigma} \frac{d \ln \Omega_K}{dr}, \quad (1)$$

where v_r is the radial velocity of gas, $\Sigma = 2I_3 \rho_0 H$ is surface density, and $W \equiv \int p_{\text{total}} dz = 2I_4 p_0 H$ is pressure integral, H is disk scale height, respectively. Here, the pressure, p_0 , and the density, ρ_0 , are related to each other by the relation $p_0 \propto \rho_0^{1+1/N}$ (the subscript ‘0’ indicates the quantities on the equatorial plane). We fixed the polytropic index to be $N = 3$, for which the numerical constants are $I_3 = 16/35$ and $I_4 = 128/315$ (Hōshi, 1977).

The specific angular momentum and the Keplerian angular momentum are defined by $\ell (= r v_\varphi)$ and $\ell_K = r^2 \Omega_K$, respectively, where Ω_K is the Keplerian angular frequency. The angular momentum conservation is

$$\dot{M}(\ell - \ell_{\text{in}}) = -2\pi r^2 T_{r\varphi}, \quad (2)$$

where \dot{M} is mass accretion rate,

$$\dot{M} = -2\pi r v_r \Sigma = \text{constant.}, \quad (3)$$

from continuity equation and $T_{r\varphi}$ is the height integrated viscous stress tensor, $T_{r\varphi} \equiv \int t_{r\varphi} dz$.

Hydrostatic balance in the vertical direction leads

$$H^2 \Omega_K^2 = (2N + 3) \frac{W}{\Sigma} = c_s^2, \quad (4)$$

where c_s is the sound speed.

The equation of state is

$$p_{\text{total}} = p_{\text{gas}} + p_{\text{rad}} = \frac{R}{\bar{\mu}} \rho_0 T_0 + \frac{a}{3} T_0^4, \quad (5)$$

where R , $\bar{\mu}$, and a are the gas constant, the mean molecular weight, and the radiation constant respectively. As to the viscosity prescription we rewrite it in terms of the effective α ;

$$T_{r\varphi} = -\alpha_{\text{eff}} W \quad \text{with} \quad \alpha_{\text{eff}} \equiv \alpha \beta^\mu = \alpha (p_{\text{gas}}/p_{\text{total}})^\mu. \quad (6)$$

This form is convenient to compare with the cases with the usual viscosity prescription (i.e., $\mu = 0$). If we take an extreme case of $\mu \rightarrow 0$ limit, the stress tensor is proportional to total pressure; i.e., the same as that of the SSD prescription. In the large μ limit ($\mu \rightarrow 1$), on the other hand, the shear stress tensor depends solely on gas pressure. This situation may realize when there grows turbulence generated by chaotic magnetic fields (Lightman, Eardley 1974; Sakimoto, Coroniti 1981).

The energy equation involves the viscous heating, radiative cooling and advective cooling terms; namely,

$$Q_{\text{vis}}^+ = Q_{\text{rad}}^- + Q_{\text{adv}}^-, \quad (7)$$

where each term is explicitly written as:

$$Q_{\text{vis}}^+ = rT_{r\varphi} \frac{d\Omega}{dr} = -r\alpha_{\text{eff}} W \frac{d\Omega}{dr}, \quad (8)$$

$$Q_{\text{rad}}^- = \frac{8acT_0^4}{3\bar{\kappa}\rho_0 H}, \quad (9)$$

and

$$Q_{\text{adv}}^- = \frac{I_4}{I_3} v_r \Sigma T_0 \frac{ds_0}{dr}. \quad (10)$$

Here, s_0 is the entropy on the equatorial plane, $\bar{\kappa}$ is the Rosseland-mean opacity, $\bar{\kappa} = \kappa_{\text{es}} + \kappa_{\text{ff}} = 0.40 + 0.64 \times 10^{23} \bar{\rho} \bar{T}^{-7/2} \text{g}^{-1} \text{cm}^2$ with $\bar{\rho}$ and \bar{T} being averaged density and temperature, respectively, ($\bar{\rho} = 16/35\rho_0$ and $\bar{T} = 2/3T_0$) and other symbols have their usual meanings. We solved the above set of equations (2)–(7). The solution is calculated from the outer edge of the disk ($r_{\text{out}} = 10^4 r_g$) to the vicinity of the central black hole through the transonic point. We adjust l_{in} , specific angular momentum which is finally swallowed by the black hole, so as to satisfy the regularity condition at the transonic radius.

For evaluating the effective temperature, we assume that all the radiative energy is emitted with blackbody as a first approximation. Namely, using the Stefan-Boltzmann's law, $Q_{\text{rad}}^- = 2F = 2\sigma T_{\text{eff}}^4$, we define the local effective temperature to be $T_{\text{eff}} = (Q_{\text{rad}}^-/2\sigma)^{0.25}$. As is widely known, however, the effect of Compton scattering is substantial in electron scattering dominated layers (Czerny, Elvis 1987; Ross et al. 1992; Shimura, Takahara 1995; Wang et al. 1999). We include this effect by introducing a spectral hardening factor (see Section. 3.3.). Further, photon trapping effect (e.g., Mineshige et al. 2000) needs to be considered. However, we ignore these effects in order to understanding the basic tendency of the spectrum.

Finally, we define the normalized parameter $\dot{m} = M/M_{\text{crit}}$, with $M_{\text{crit}} = L_E/c^2 = 1.3 \times 10^{17} (M/M_\odot) \text{g s}^{-1}$. This definition may differ in different literatures. In our notation, disk luminosity corresponds to the Eddington luminosity, when the accretion rate is $\dot{m} = 16$ (provided that the pseudo-Newtonian potential is used). We vary the normalized parameters, $m \equiv M/M_\odot$, \dot{m} , α , and μ , and calculate the structure of optically thick accretion disk for a wide range of parameters.

3. The effects of varying viscosity prescriptions

3.1. The α -Dependence

We first examine the effects of changing the α parameter within the SSD prescription, $t_{r\varphi} = -\alpha p_{\text{total}}$, i.e., $\mu = 0$. It is well known that α does not affect significantly the spectrum in the standard disk theory, since total radiation output rate is balanced with the energy generation rate via viscous processes and does not explicitly depend on density nor velocity. In other words, effective temperatures can be nearly uniquely determined by black-hole

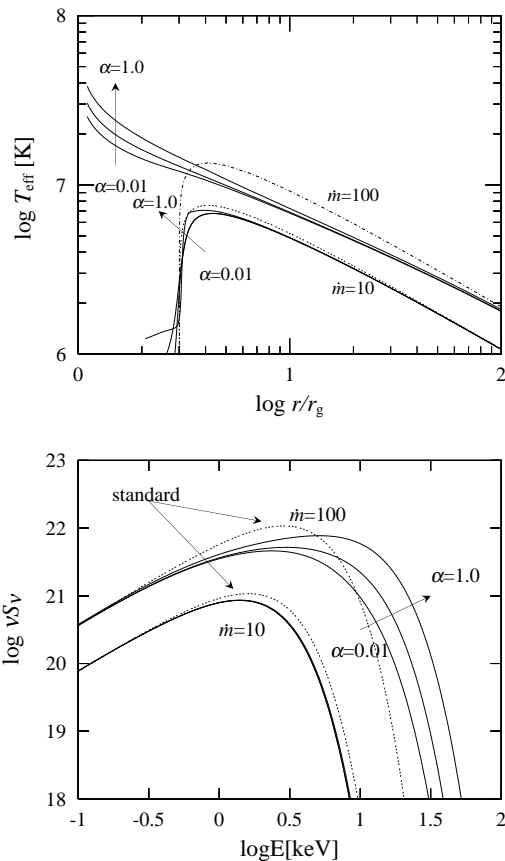


Fig. 1. The effective temperature distributions and the emergent spectra for different α parameters ($\alpha=0.01, 0.1$, and 1.0). Solid lines represent the calculated models (for $\dot{m} = 10$ and 100). Dashed lines are the results based on the standard-disk relation (Shakura, Sunyaev 1973). For a small accretion rate, $\dot{m} = 10$, the spectrum does not largely depend on α parameter, whereas at a high accretion rate, $\dot{m} = 100$, α dependence appears in the temperature profile in the inner region. Likewise, the spectral changes are not appreciable in the case of $\dot{m} = 10$ while in $\dot{m} = 100$ case, the spectrum has α dependence reflecting the α dependence of the temperature distribution. Black-hole mass is fixed to be $10M_\odot$.

mass and mass-accretion rate as functions of radius. In a high accretion-rate system, in contrast, α dependence appears, since radiative cooling is no longer balanced solely with viscous heating so that the disk inner temperature can change even for the same M and \dot{M} .

Figure 1 shows the temperature profiles and spectra for different α and \dot{m} . In the temperature profiles, we found $T \propto r^{-3/4}$ at low $\dot{m} \lesssim 10$ (called as the SSD regime) and $T \propto r^{-1/2}$ at large $\dot{m} \gtrsim 100$ (called as the slim-disk regime, see Watarai, Fukue, 1999, Watarai et al. 2000; Wang et al. 1999). For instance, when α increases by one order of magnitude, the temperature in the vicinity of the disk inner region only slightly rises by a factor of ~ 2 , and X-ray radiation spectra get a bit harder.

Next, we check the relative importance of advective energy transport in the energy equation. Figure 2 plots the ratio, $Q_{\text{adv}}^-/Q_{\text{vis}}^+$, for different α and \dot{m} . When α increases,

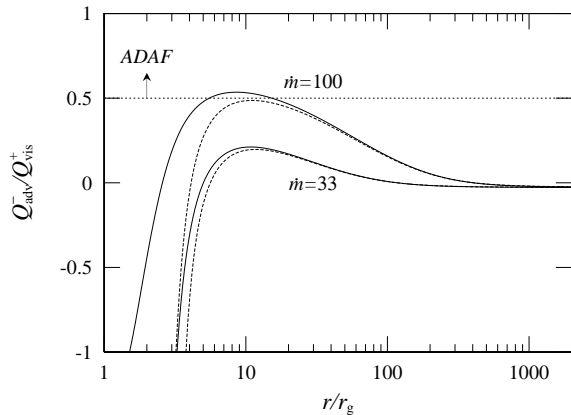


Fig. 2. The ratio of advective energy transport to the viscous heating rate for different accretion rate ($\dot{m}=33$ and 100). For all the cases, the viscous heating rate Q_{vis}^+ is balanced with the radiative cooling Q_{rad}^- at larger radii, thus $|Q_{adv}^-| \ll Q_{vis}^+$. At higher accretion rates, the advective cooling Q_{adv}^- is substantial at inner radii, but still, the ratio is mostly less than 0.5; that is, the flow is not advection dominated. Black-hole mass is fixed to be $M = 10M_{\odot}$, and we set $\alpha = 0.1$ (the solid lines) and 0.01 (the dotted lines).

this ratio also increases; that is, the large α is, the more effectively advection cooling works. We note, however, that even for $\dot{m} = 100$, still disk is not entirely advection dominated (the maximum ratio is ~ 0.5). Thus, it is not appropriate to call the slim disk the optically thick ADAF (see also Abramowicz et al. 1988).

Figure 1 explicitly demonstrates that the disk inner edge decreases as \dot{m} increases. Why, then, can the inner edge of the disk be smaller than the radius of the marginally stable circular orbit, $r_{ms} \sim 3r_g$? One of the reasons is a decrease of the transonic radius of the flow, r_S , ($r_S \lesssim r_{ms}$) with increase of accretion rate; i.e. $r_S/r_g = 3.00$, 2.84 and 2.69 for $\dot{m} \leq 10, 33$ and 100, respectively. We obtained r_S for several \dot{m} and confirmed that the tendency of r_S is consistent with that of Abramowicz et al. (1988). In the case of super-critical accretion, moreover, a pressure gradient force is important as in the case of a thick torus (Abramowicz et al. 1978). For small α (< 0.1) accretion is, in fact, driven by pressure gradient. Then, the pressure gradient force tend to push material near the inner edge of the disk inward to smaller radii, even if the material has larger angular momentum than the equilibrium value, for which centrifugal force is balanced with gravity force. Finally, even when the flow is unstable for circular motion, the growth time is on the order of free-fall accretion time, while in the meantime mass is continuously supplied from outside with large (comparable to sound) velocity at large \dot{m} . There always exists substantial material inside r_{ms} , emitting radiation.

For large α value (~ 1.0) the accretion is driven by the viscosity, however, such a flow can be effectively optically thin. It was pointed out by Beloborodov (1998) that in the case of very large $\alpha \sim 1.0$, the inner region of the disk may be overheated due to decreasing the effective optical

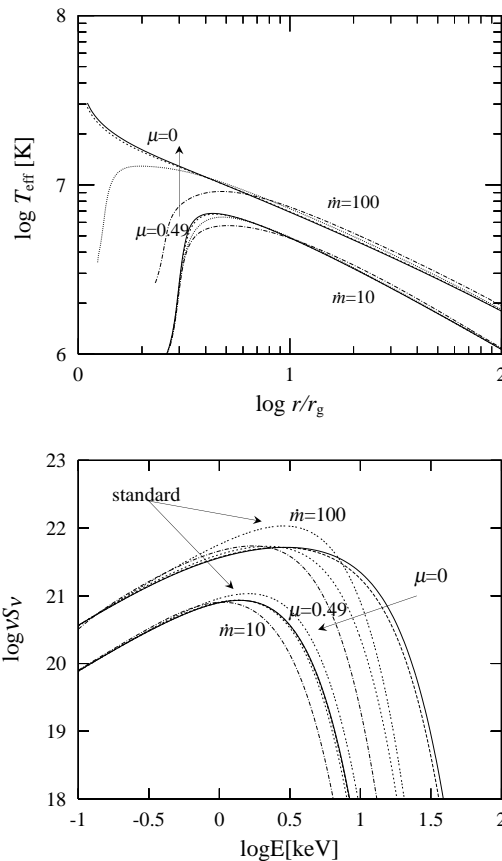


Fig. 3. The same as figure 1 but different μ parameters ($\mu = 0, 0.1, 0.4$, and 0.49).

depth, but strong convective motion will reduce thermalization timescale, which may avoid overheated problem for moderately large $\alpha \sim 0.1$ (Mineshige et al. 2000).

3.2. The μ Dependence

In this subsection, we discuss the μ dependence of the slim disk structure. In equation (6), we fix α ($=0.1$) and M ($=10M_{\odot}$) but change the value of μ ($=0, 0.1, 0.4$, and 0.49). If we take the limit of μ approaching unity; that is $t_{r\varphi} = -\alpha p_{gas}$, and then the disk will be completely stabilized, since then temperature dependence of the heating rate ($\propto t_{r\varphi}$) is now less than that of the cooling term, a condition for thermal stability (see Kato et al. 1998, Chap. 4).

Figure 3 display the temperature profiles and the spectra for different μ values. When $\dot{m} = 10$, the temperature does not show μ dependence. In the $\dot{m} = 100$ case, in contrast, the temperature appreciably decreases around transonic region ($< 3r_g$) as μ decreases, keeping the same temperature slope, $T \propto r^{-1/2}$, at large radii, $r \gg 3r_g$.

The basic interpretations of these results are that a large μ tends to decrease α_{eff} at smaller radii, thus decelerating infall motion of gas into black hole. This rather promotes radiative cooling, thereby decreasing temperature. This means, the parameter μ more appreciably affects the flow

structure in the vicinity of the central hole.

3.3. Observable μ effects

Finally, we show the effects of changing μ more explicitly in the model spectral fitting diagram in comparison with the observational properties of soft X-ray dominated sources. The method of model fitting is the same as that described in Mineshige et al. (1994; see also Watarai et al. 2000). The fitting parameters are $R_{\text{in}}^{\text{mod}}$, which determines the height of the spectral peak, $T_{\text{in}}^{\text{mod}}$, specifying the frequency of the spectral peak, and the power-law index in the temperature distribution, “ p ” ($\equiv -d\ln T/d\ln r$), which controls the spectral slope at low-energy (the Rayleigh-Jeans) side of the peak. We thus assume the form,

$$S(E) \propto \int_{T_{\text{in}}^{\text{mod}}}^{T_{\text{out}}^{\text{mod}}} \left(\frac{T}{T_{\text{in}}^{\text{mod}}} \right)^{-2/p-1} B(E, T) \frac{dT}{T_{\text{in}}^{\text{mod}}}, \quad (11)$$

where $T_{\text{out}}^{\text{mod}}$ is the temperature at the outer edge and $B(E, T)$ is the Planck function. The limit of $p \sim 0.75$ corresponds to the original MCD model, while $p \sim 0.5$ indicates the typical temperature gradient of the slim disk model, $T \propto r^{-1/2}$. The results of the fitting for different μ values are summarized in Tables 1–3 (see also Tables 4 and 5 for different α cases). Throughout this section, we fix $\alpha = 0.1$. Note that we are more concerned with relative changes of the fitting parameters as functions of M and \dot{M} , rather than their absolute values for specific values of M and \dot{M} , since realistically, general relativistic effects and other effects (such as self-shielding and the disk tilting) should modify the results, which are not easy to evaluate precisely. However, general tendency does not change as long as the central black hole is non-rotating (see Manmoto, Mineshige 2001 for the detailed discussion).

According to our previous paper (Watarai et al. 2001), the “ $T_{\text{in}}^{\text{obs}} - R_{\text{in}}^{\text{obs}}$ ” diagram is useful for diagnosing the objects having a soft thermal component in the X-ray spectrum; with this we can constrain various models (see also Belloni 2000, Mizuno et al. 2000). We considered the spectral hardening factor, ξ (Shimura, Takahara 1995), and the correlation factor, η (Kubota et al. 1998), in the fitting results. The hardening factor ξ represents the spectral hardening due to Comptonization processes within the disk ($T_{\text{in}}^{\text{obs}} = \xi T_{\text{in}}^{\text{mod}}$, see the second column of tables). The η parameter is introduced, since the radius of the apparent inner edge, $R_{\text{in}}^{\text{mod}}$ derived by spectral fitting based on equation (11) is generally overestimated by a factor of few because of negligence of the boundary term, so as to remove such artificial effects and to evaluate the radius of the real inner edge ($R_{\text{in}}^{\text{obs}} = \eta R_{\text{in}}^{\text{mod}}$, see the fourth column of tables). In this paper, we set $(\xi, \eta) = (1.7, 0.41)$ according to Kubota et al. (1998). The “ $T_{\text{in}}^{\text{obs}} - R_{\text{in}}^{\text{obs}}$ ” diagram are shown in Fig 4.

In the cases with $\mu = 0.01$, the fitting results are nearly consistent those with $\mu = 0$. As μ increases, $R_{\text{in}}^{\text{obs}}$ decreases (see Tables 1–3). For $\mu > 0.4$, in particular, the inner disk temperature can never be larger than 2.0 keV. As we described in the previous section, when the effective

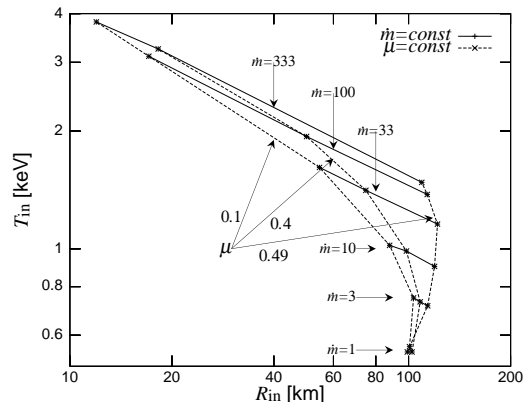


Fig. 4. The fitting parameters $T_{\text{in}}^{\text{obs}}$, $R_{\text{in}}^{\text{obs}}$ are plotted in this figure. The black-hole mass is $M = 10M_{\odot}$. The solid lines are $\dot{m} = \text{const.}$ and the dotted lines are $\mu = \text{const.}$, respectively.

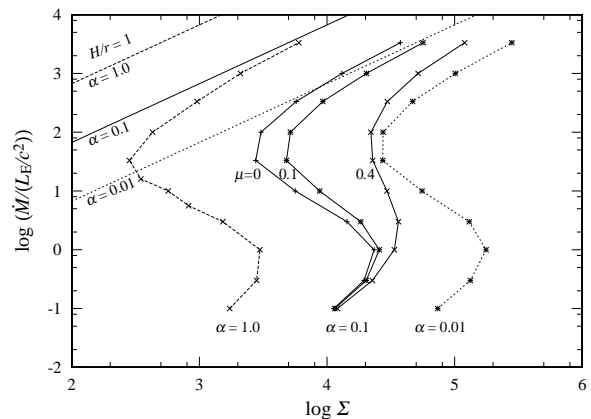


Fig. 5. The thermal equilibrium (S-shaped) curves for different parameter sets; $(\alpha, \mu) = (1.0, 0.0)$, $(0.1, 0.0)$, $(0.1, 0.1)$, $(0.1, 0.4)$, and $(0.01, 0.0)$, respectively. The abscissa is the normalized mass accretion rate, and the ordinate is the surface density both on the logarithmic scale. The dashed-dotted lines represent the loci of $H/R = 1$ for several value of α .

α is large, the disk cannot release its gravitational energy efficiently even for $\dot{m} = 100$.

It is difficult to discriminate different models from the observational fitting results in Fig 4, because the difference between $\mu = 0$ and 0.4 is only a factor of a few. In the case of smaller \dot{m} value, there is practically no change. When \dot{m} is large, $\dot{m} \gtrsim 30$, on the other hand, $T_{\text{in}}^{\text{obs}}$ changes by factor of a few, and $R_{\text{in}}^{\text{obs}}$ changes by one order of magnitude, depending on μ values.

4. Discussion

We thus expect different time-dependent behavior of a single source, depending on the μ values, if large \dot{m} modulation is observed. In the case of $\mu \sim 0.5$, importantly, the disk inner radius $R_{\text{in}}^{\text{obs}}$ does not change much even when \dot{m} changes a lot, in contradiction with the observed behavior of IC 342 which clearly shows a decrease in $R_{\text{in}}^{\text{obs}}$ when

L increases (Watarai et al. 2001). Thus, the case with $\mu \sim 0.5$ can be ruled out at least for the case of ULXs.

According to the SSD theory, the α parameter affects the flow velocity (v_r) and thus matter density (Σ), in such a way that mass-flow rate ($\propto v_r \Sigma$) is kept constant, but does not largely affect its local emitting flux (as long as a simple blackbody radiation is assumed). In the high accretion-rate systems, however, the temperature within the transonic region of the flow is directly affected by the α value. Unlike the SSD the thickness of the high-luminosity disk becomes mildly thick (the relative thickness H/R is less than but of order unity) and Thomson optical depth is quite large. Therefore, photons generated by viscosity take longer time to reach the disk surface than the accretion timescale so that the generated energy by viscosity cannot be radiated immediately.

From the observational point of view, the “ μ ” parameter acts more effectively on the fitting parameters in the slim disk than in the standard disk. This result leads the conclusion that the super-Eddington sources are useful for investigating the nature of viscosity. We find that, even if objects have truly high accretion rates, they may look like a standard-type disk, if μ is large. If we accurately measure the change in $R_{\text{in}}^{\text{obs}}$ with changes of \dot{m} , we will be able to give a good estimate to the μ value.

The origin of the viscosity in accretion disk is still poorly known, so it is practically impossible at the present to constrain the value of μ from the first principle. Also, the observational determination of μ is not easy. If μ has a larger value in reality, the disk does not enter the advection-dominated regimes, even if the super-critical accretion is realized. The results of the present study are useful for constraining the viscosity model. For example, large μ (> 0.1) models do not agree with the observed properties of ULXs, which show a tendency of decreasing $R_{\text{in}}^{\text{obs}}$ ($\lesssim 3r_g$) at large luminosity (Watarai et al. 2001). Hence, the viscosity model with a large μ parameter can be ruled out for such sources.

Figure 5 illustrates the thermal equilibrium curves of the calculated disk at a fixed radius ($r = 7r_g$). The straight lines in the upper-left corner of the figure represent the loci of $H/r = 1$ for several values of $\alpha = 0.01, 0.1, \text{ and } 1.0$ from the bottom, respectively. How close the equilibrium curve is to the line of $H/r = 1$ is a good indicator to assess how the advection is important in energy equation, since $Q_{\text{adv}} \gtrsim (H/r)^2 Q_{\text{vis}}$ (Kato et al. 1998). The relative distance between the upper branch of the S-shaped curve and the line of $H/r = 1$ hardly changes for each set of the same α in Fig 5. On the other hand, it is clearly demonstrated that when μ is large, the kinks are not strongly manifested. Limit-cycle oscillations can occur at high \dot{m} , only when μ is small, and the amplitudes of oscillations decreases as μ increases (Honma et al. 1991; Szuszkiewicz, Miller 1997, 1998). Large μ values tend to stabilize the disk structure so that for even higher μ ($\gtrsim 0.5$) the limit cycle oscillations cannot occur.

The occurrence of limit-cycle oscillations in real systems is still in open question. There is a hint of such oscillation in GRS1915+105 (Yamaoka et al. 2001), but we need

careful data analysis in future work.

The complementary work to the present study is made by Manmoto, Mineshige (2001) who consider fully relativistic treatments of the slim-disk problem but only for the canonical viscosity prescription ($t_{r\phi} = -\alpha p_{\text{tot}}$) with $\alpha = 0.1$. Main results are: (i) for the disk around a Schwarzschild black hole $R_{\text{in}}^{\text{obs}}$ decreases from $3r_g$ to $\sim 1.5r_g$ as mass-accretion rate increases beyond a critical value $\dot{M}_{\text{crit}} \sim 30L_E/c^2$; (ii) for the disk around a Kerr hole (KBH), conversely, $R_{\text{in}}^{\text{obs}}$ increases from $< r_g$ to $\sim 1.5r_g$ as mass-accretion rate increases because of significant self-shielding of the innermost hot region; (iii) at accretion rate above the critical value, disks around Schwarzschild and Kerr holes look quite similar; (iv) in both cases, the temperature distribution is somewhat flatter, $\propto r^{-1/2}$, at large luminosity. These results are basically in good agreement with the present study based on the pseudo-Newtonian treatment (except for the case of Kerr holes which are not considered here), but there exist some quantitative differences. In the present study, hence, we are more concerned with the qualitative trend and thus it is unlikely that our main conclusions significantly change, even if fully relativistic treatments expect that very small $R_{\text{in}}^{\text{obs}} < r_g$ may be an artifact of our pseudo-Newtonian treatments.

For more realistic study along this line we also need fully 2D studies, taking into account the radiative transfer towards the vertical direction and various MHD processes. This is left as future work. Time dependent modeling of bursting behavior observation GRS1915+105 is another interesting subject in future work.

Recently, King et al. (2001) proposed that large L and high $T_{\text{in}}^{\text{obs}}$ observed in ULXs could be understand, if X-ray is moderately beamed. We suggest that spectral fitting with the *p-free model* will be able to test this hypothesis, since it only the thermal emission from the innermost region is beamed, the resultant spectrum will be of a single-temperature blackbody; i.e., large p will be obtained. Otherwise, we expect $0.5 \leq p \leq 0.75$. We can thus judge it beaming is substantial in future observations (with, e.g., XMM Newton).

5. Conclusions

We have discussed the properties of the slim disk for different viscosity prescriptions and their soft X-ray signatures. Our conclusions are summarized as below.

1. Some α dependence is found in the radial temperature distribution of the innermost region of high accretion-rate systems ($\dot{m} \gtrsim 30$); an increase in α tends to increase the temperature of the transonic flow, making a spectrum somewhat harder, although the change is not large and thus not easy to detect observationally.
2. When the parameter μ takes a larger value (e.g. $\mu = 0.5$), the slim-disk nature (small $R_{\text{in}}^{\text{obs}} \lesssim 3r_g$ and flatter temperature profile, $T_{\text{eff}} \propto r^{-1/2}$) is not appreciable even at high luminosity comparable to the Eddington luminosity.

3. The origin of the viscosity is still unknown, but observations of high luminosity objects will be able to discriminate different viscosity prescriptions for accretion disks. For example, large μ values are not incompatible with the behavior of some ULXs. The viscosity should thus be more dependent on total pressure, rather than gas pressure solely.

We are grateful to the referee, E. Szuszkiewicz, for pointing out the initial of errors in the first version and for useful comments and discussion, which helped our making the revised version. We would also like to thank M. Takeuchi and T. Kawaguchi for discussion. This work was supported in part by the Grants-in Aid of the Ministry of Education, Science, Sports, and Culture of Japan (13640238, SM).

References

- [Abramowicz, M.A., Jaroszyński, M., Sikora, M. 1978, A&A, 63, 221
- [Abramowicz(1995)] Abramowicz, M.A., Chen, X., Kato, S., Lasota, J.P., Regev, O. 1995, ApJL, 438, L37
- [Abramowicz(1988)] Abramowicz, M.A., Czerny, B., Lasota, J.P., Szuszkiewicz, E. 1988, ApJ, 332, 646
- [Beloborodov(1998)] Beloborodov, A.M. 1998, MNRAS, 297, 739
- [Belloni, T., Migliari, S., Fender, R.P. 2000, A&A, 358, L29
- [Chen, X., Taam, R.E. 1993, ApJ, 412, 254
- [Czerny, B., Elvis, M. 1987, ApJ, 321, 305
- [Fabbiano, G. 1989, A&ARev., 27, 87
- [Fukue(2000)] Fukue, J. 2000, PASJ, 52, 829
- [Honma et al(1991)] Honma, F., Matsumoto, R., Kato, S. 1991, PASJ, 43, 147
- [Honma et al(1991)] Honma, F., Matsumoto, R., Kato, S., Abramowicz, M.A. 1991, PASJ, 43, 261
- [Hōshi, R. 1977, *Prog.Theor.Phys.*, 58, 1191
- [Kato(1998)] Kato, S., Fukue, J., Mineshige, S. 1998, *Black-Hole Accretion Disks* (Kyoto University Press, Kyoto)
- [king(2001)] King, A.R., Davies, M.B., Ward, M.J., Fabbiano, G., Elvis, M. 2001, ApJL, 552, L109
- [kubota(1998)] Kubota, A., Tanaka, Y., Makishima, K., Ueda, Y., Dotani, T., Inoue, H., Yamaoka, K. 1998, PASJ, 50, 667
- [Laor, A., Netzer, H., 1989, MNRAS, 238, 897
- [Lightman, A.P., Eardley, D.M. 1974, ApJL, 187, L1
- [Lin, D.N.C., Shields, G.A., 1986, ApJ, 305, 28
- [Makishima(2000)] Makishima, K., Kubota, A., Mizuno, T., Ohnishi, T., Tashiro, M., Aruga, Y., Asai, K., Dotani, T., Mitsuda, K., Ueda, Y., Uno, S., Yamaoka, K., Ebisawa, K., Kohmura, Y., Okada, K. 2000, ApJ, 535, 632
- [Manmoto, T., Mineshige, S. 2001, in preparation
- [Matumoto(1984)] Matsumoto, R., Kato, S., Fukue, J., Okazaki, A. 1984, PASJ, 36, 71
- [Mineshige et al.(2000)] Mineshige, S., Kawaguchi, T., Takeuchi, M., Hayashida, K. 2000, PASJ, 52, 499
- [Paczynski (1980)] Paczyński, B., Wiita, P.J. 1980, A&A, 88, 23
- [Ross et al.(1992)] Ross, R.R., Fabian, A.C., Mineshige, S. 1992, MNRAS, 258, 189
- [Sakimoto, P.J., Coroniti, F.V. 1981, ApJ, 247, 19
- [Shakura & Sunyaev.(1973)] Shakura, N.I., Sunyaev, R.A. 1973, A&A, 24, 337
- [Shimura et al.(1995)] Shimura, T., Takahara, F. 1995, ApJ, 445, 780
- [Szuszkiewicz, E. 1990, MNRAS, 244, 377
- [Szuszkiewicz et al.(1996)] Szuszkiewicz, E., Malkan, M.A., Abramowicz, M.A. 1996, ApJ, 458, 474
- [Szuszkiewicz, E., Miller, J. C. 1997, MNRAS, 287, 165
- [Szuszkiewicz, E., Miller, J. C. 1998, MNRAS, 298, 888
- [Taam, R.E., Lin, D.N.C. 1984, ApJ, 287, 761
- [Wang, J.M., Szuszkiewicz, E., Lu, F.J., Zhou, Y.Y., 1999, ApJ, 522, 839
- [Watarai(1999)] Watarai, K., Fukue, J. 1999, PASJ, 51, 725
- [Watarai(2000)] Watarai, K., Fukue, J., Takeuchi, M., Mineshige, S. 2000, PASJ, 52, 133
- [Watarai, K., Mizuno, T., Mineshige, S. 2001, ApJL, 549, 77
- [Yamaoka et al. 2001, in the New Century of X-ray Astronomy
- [Zampieri, Turolla, T., Szuszkiewicz, S. 2001, MNRAS, 325, 1266

Table 1. Results of fitting with p -free model (0.2-10keV). ($M = 10M_{\odot}$, $\mu = 0.1$, $\alpha = 0.1$)

$\bar{M}/(L_E/c^2)$	$T_{\text{in}}^{\text{obs}}$ (keV)	$R_{\text{in}}^{\text{mod}}$ (km)	$R_{\text{in}}^{\text{obs}}/r_g$	p
1	0.56 (0.2-8.0 keV)	245.4	3.35	0.75
3	0.75	237.1	3.24	0.74
10	1.02	211.0	2.88	0.72
33	1.60	142.1	1.78	0.68
100	2.86	56.7	0.77	0.61
333	3.37	40.1	0.55	0.58

Table 2. Results of fitting with p -free model ($M = 10M_{\odot}$, $\mu = 0.4$, $\alpha = 0.1$)

$\bar{M}/(L_E/c^2)$	$T_{\text{in}}^{\text{obs}}$ (keV)	$R_{\text{in}}^{\text{mod}}$ (km)	$R_{\text{in}}^{\text{obs}}/r_g$	p
1	0.54 (0.2-5.0keV)	249.6	3.41	0.75
3	0.75	247.0	3.37	0.74
10	0.99	233.5	3.19	0.73
33	1.39	200.1	2.73	0.71
100	1.90	138.1	1.89	0.65
333	2.92	63.8	0.87	0.59

Table 3. Results of fitting with p -free model ($M = 10M_{\odot}$, $\mu = 0.49$, $\alpha = 0.1$)

$\bar{M}/(L_E/c^2)$	$T_{\text{in}}^{\text{obs}}$ (keV)	$R_{\text{in}}^{\text{mod}}$ (km)	$R_{\text{in}}^{\text{obs}}/r_g$	p
1	0.54 (0.2-8.0keV)	241.77	3.36	0.74
3	0.73	266.24	3.69	0.76
10	0.90	290.92	4.04	0.75
33	1.16	296.76	4.10	0.73
100	1.38	276.28	3.83	0.68
333	1.48	266.66	3.07	0.62

Table 4. Results of fitting with p -free model ($M = 10M_{\odot}$, $\mu = 0$, $\alpha = 0.01$)

$\bar{M}/(L_E/c^2)$	$T_{\text{in}}^{\text{obs}}$ (keV)	$R_{\text{in}}^{\text{mod}}$ (km)	$R_{\text{in}}^{\text{obs}}/r_g$	p
1	0.56 (0.2-8.0keV)	245.4	3.41	0.75
3	0.73	236.4	3.28	0.74
10	1.04	207.0	2.87	0.71
33	1.51	153.5	2.13	0.68
100	2.50	68.64	0.95	0.61
333	2.94	51.59	0.72	0.57

Table 5. Results of fitting with p -free model ($M = 10M_{\odot}$, $\mu = 0$, $\alpha = 1.0$)

$\bar{M}/(L_E/c^2)$	$T_{\text{in}}^{\text{obs}}$ (keV)	$R_{\text{in}}^{\text{mod}}$ (km)	$R_{\text{in}}^{\text{obs}}/r_g$	p
1	0.56 (0.2-8.0keV)	244.2	3.39	0.75
3	0.75	234.9	3.26	0.74
10	1.04	204.0	2.83	0.71
33	3.09	46.04	0.64	0.65
100	3.93	36.82	0.51	0.62
333	4.18	30.67	0.43	0.58